Proceedings of ASME Turbo Expo 2023
Turbomachinery Technical Conference and Exposition
GT2023
June 26-30, 2023, Boston, Massachusetts, USA

GT2023-101245

MODELLING OF TWO-PHASE WATER EJECTOR IN RANKINE CYCLE HIGH TEMPERATURE HEAT PUMPS

Omar Abu Khass*, Anh Phong Tran, Steffen Klöppel, Panagiotis Stathopoulos

German Aerospace Center, Institute of Low-Carbon Industrial Processes, Cottbus/Zittau, Germany

ABSTRACT

Industrial high temperature heat pumps (HTHPs) can provide carbon-free process heat when operated with renewable energy sources. Using water as the working medium greatly increases the possible range of operation without the detrimental effects of traditional working fluids. One main challenge with this type of heat pump is the high compression ratio required to achieve a given temperature lift. As a result, water based heat pumps need several compression stages. Furthermore, the steam leaving the compressor is highly superheated. Ejectors driven by high pressure condensate allow to de-superheat the steam from the compressor outlet while simultaneously increasing its pressure. Thereby, the required power for compression as well as the number of compression stages can be reduced. This paper studies how the implementation of the two-phase water ejector influences the thermodynamic performance of Rankine cycle HTHP using a thermodynamic model of the ejector. Several cycle architectures are developed to study the ejector integration in the heat pump cycle, including traditional single-stage and multi-stage cycles. The cycles studies are conducted in the Modelica language, in the Modelon Impact environment. The study aims at informing about new developments in two-phase water ejectors and their application potential in Rankine cycle HTHPs. First simulations suggest an efficiency improvement of about 10 % *through the use of an ejector in the heat pump cycle.*

Keywords: Ejector, High temperature heat pumps, Rankine cycle heat pump, Industrial process heat, Steam compression

NOMENCLATURE

Roman letters

A	Area [m^2]
a_{cr}	Critical speed of sound [$m\ s^{-1}$]
c	Velocity [$m\ s^{-1}$]
COP	Coefficient of performance
HTHP	High temperature heat pump
GWP	Global warming potential
h	Enthalpy [$J\ kg^{-1}$]
$\dot{m}$	Mass flow rate [$kg\ s^{-1}$]
M	Mach number [-]
ODP	Ozone depletion potential
P	Power [W]
p	Pressure [Pa]
s	Entropy [$J\ kg^{-1}\ K^{-1}$]
T	Temperature [K]
w	Entrainment ratio [-]
x	Quality [-]

Greek letters

η	Efficiency [%]
κ	Isentropic exponent [-]
ν	Specific volume [$m^3\ kg^{-1}$]
Π	Pressure ratio [-]
ρ	Density [$kg\ m^{-3}$]

Superscripts and subscripts

as	After shock wave
bs	Before shock wave
c	Compressor
diff	Diffuser
e	Electrical
ej	Ejector
is	Isentropic
mc	Mixing chamber
mn	Motive nozzle
mot	Motive fluid
opt	Optimum
p	Pump
s	Steam
sn	Suction nozzle
sup	Superheat
suc	Suction fluid
tot	Total

*Corresponding author: omar.abukhass@dlr.de

1. INTRODUCTION

In the path towards the reduction of CO_2 emissions, the industrial sector plays a crucial role. In the European industry, 66 % of the total final energy demand are used for process heating [1]. Many processes require heat above 150 °C, which is usually provided by burning fossil fuels. To avoid the associated CO_2 emissions, innovative and sustainable technologies for providing process heat have to be developed. When operated with renewable electricity, industrial high temperature heat pumps (HTHPs) can provide carbon-free process heat. HTHPs are highly attractive energy conversion devices that offer efficient means to reduce primary energy consumption of industrial processes by utilizing waste heat recovery [2]. However, commercially available heat pumps can usually operate up to temperatures of 150 °C [2]. In order to achieve higher temperatures with heat pumps, further research and development is necessary. One concept is currently being developed at the German Aerospace center (DLR) based on the reverse Rankine process with water (R718) as the working fluid [3]. Using water as the working fluid greatly increases the possible range of operation without the detrimental effects of traditional working fluids. Water is a natural refrigerant with zero global warming potential (GWP) and zero ozone depletion potential (ODP). It is neither toxic nor flammable and it has a high critical temperature of 374 °C. In fact, the latent heat of water is very high, making it very attractive for use in temperatures above 150 °C [2, 4]. This will in return provide a large market potential for their use in industrial sectors such as pulp & paper, chemical, food and even the iron industry [2]. However, two main challenges associated with water are the low density of its vapor phase and its steep boiling curve. As a consequence, the required swept volume and pressure ratio is typically high for heat pump applications. That is why several compressor stages with intermediate cooling are needed to achieve the required discharge temperature and pressure [2].

In the recent years, several efforts were and are still being made to develop new compressor technologies for steam compression. Among them are the high-speed oil-free turbo compressors with high flow rates to compensate for the low density of water vapor. However, the low-pressure ratio and relatively high cost of such compressors puts a barrier in their wider use in the market [2]. This dictates the needs for further research on efficient water compression technologies and at the same time, the need for alternative compression technologies in addition to compressors for the use in water HTHPs. Ejectors driven by high pressure condensate allow to de-superheat the steam from the compressor outlet, while simultaneously increasing its pressure. Thereby, the required power for compression as well as the number of compression stages can be reduced for a given temperature lift of the heat pump.

Ejectors have been widely studied. Fundamental studies on the theory of gas and steam ejectors can be found for example in the work of Power 1993 [5]. Thorough reviews on the applications of ejectors in refrigeration systems can be found in following references [6, 7]. A theoretical and experimental study of two-phase ejectors applied in the compressor refrigeration systems as devices to reduce the throttling losses, or as second step compression in refrigeration cycles is presented by [8–10]. Two-phase ejectors are also used in CO_2 (R744) systems due to the high exergy loss in the respective throttling process. Elbel and Hrnjak [10] have carried out experimental work on the use of two-phase ejectors in a transcritical R744 vapor jet refrigeration cycle. Their work revealed that the efficiency of the ejector-equipped R744 heat pump system could increase by 8 % in comparison to a system without an ejector. However, there is only a handful of publications on two-phase ejectors with water as the working fluid [11, 12].

Šarevski and Šarevski [11] developed a R718 refrigeration system with a single stage centrifugal compressor and a two-phase ejector as a second stage compression device. Vapor from centrifugal compressor directly comes into the two-phase ejector, where it mixes with high pressure condensate. Complex thermal and flow phenomena occur with additional compression, de-superheating and condensation in the two-phase ejector. The rest of the system consists of an evaporator and condenser with flash evaporation and condensation. The authors presented modeling procedures for the compressor and the two-phase ejector. The work of Šarevski and Šarevski have been extended and published in 2017 [13].

The purpose of this work is to investigate how the implementation of a two-phase water ejector influences the performance of a vapor compression cycle HTHP. The cycle with the ejector will be compared to an equivalent heat pump cycle with direct water injection intercooling. The cycle studies are conducted in the Modelica language [14], utilizing the Modelon Impact environment [15]. The properties of two-phase water are modeled with the standard water media in Modelica [16]. An in house designed python tool is combined with the Modelica simulation for optimizing the ejector's performance.

2. SYSTEM DESCRIPTION

The investigated heat pump cycles are shown in Fig. 1 and Fig. 2, respectively. Addressing the cycle in Fig. 1 first, it consists of a compressor, a de-superheater and a pump for the operation of the de-superheater. The de-superheater works by injecting a small amount of pressurized water in the main steam flow. This water evaporates and reduces the temperature of the main steam flow. The second cycle, Fig. 2, consist of a compressor and has an ejector in combination with a separator. The function of the ejector here is to replace a second compressor, while achieving the same pressure at the outlet. A pump is also needed for the operation of the ejector, though the type of the pump here differs from the one needed for the operation of the de-superheater as to what will be later described. The two heat pump models represent the implementation of an open heat pump integration in an industrial partner plant. The industrial plant has a steam network with various pressures and temperatures. Certain processes at the industrial site produce steam as a waste heat which is used in the simulations here as a heat source and consequently as a direct input to the compressor. The outlet of the cycles in Fig. 1 and. 2 produces steam of higher pressure and temperature values which can be used at other positions in the plant steam network.

The cycles performance will be assessed in two areas, first area concerns the performance of the ejector and the second area addresses the performance of the whole cycle. The coefficient of

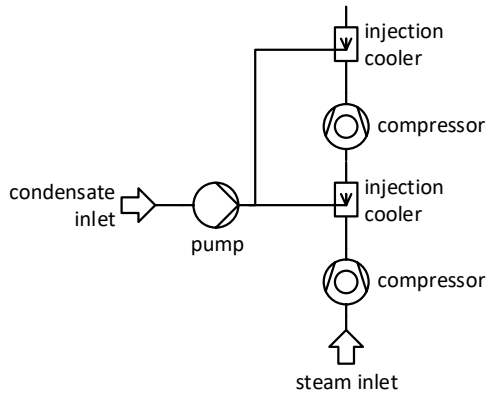

FIGURE 1: TWO STAGE COMPRESSION OPEN HEAT PUMP WITH DIRECT INJECTION COOLING

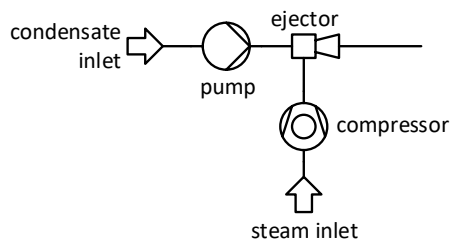

FIGURE 2: OPEN HEAT PUMP WITH AN EJECTOR AS A SECOND STEP COMPRESSION

performance (COP) will be used to assess the total efficiency of each cycle. The COP is defined as:

$$COP = \frac{\dot{Q}_{\text{sink}}}{\sum P_{\text{e}}} \tag{1}$$

where $\dot{Q}_{\text{sink}}$ is the heat flow to the heat sink and $\sum P_{\text{e}}$ is the sum of the electrical power consumption of the compressor(s) and the water pump.

The heat source thermal capacity (power) is fixed while the amount of heat delivered to the industrial plant varies depending on the cycle performance. The selected design specifications and constrains for the simulations scenarios are shown in Table 1. The compressors are simulated with an isentropic efficiency of 70 % and a pressure ratio in the range of 1.7 – 2.5 each. The values of efficiency and pressure ratios are in accordance with values provided by literature on water-based heat pumps [4, 17]. The water pump is simulated with an efficiency of 80 % as released by water pump manufacturers [18].

Water condensate is available at the industrial plant as an outcome of several processes. Usually, the condensate is returned at atmospheric pressure. Because of certain heat losses, its temperature will be below 100 °C. Here, a temperature of 90 °C is assumed. For the direct injection cycle, this water is used as a fluid for inter-stage cooling. A water pump is used to increase the water pressure to 20 bar before it flows into the de-superheater. A degree of superheating of ΔT_{sup} = 10 K is present as a constraint at the exit of the de-superheater before the inlet of the second

TABLE 1: SELECTED DESIGN SPECIFICATIONS AND CONSTRAINTS

State/Component	Imposed constraints
Steam inlet	p=1 bar(a)
	T= 100 °C
	$\dot{m}_{\text{s}}$ = 1 kg s^{-1}
Condensate inlet	p=1 bar(a)
	T = 90 °C
Compressor isentropic efficiency	$\eta_{\text{is,c}}$ = 70 %
Pump isentropic efficiency	$\eta_{\text{is,p}}$ = 80 %
Compressor pressure ratio	Π_{c} = 1.7-2.5

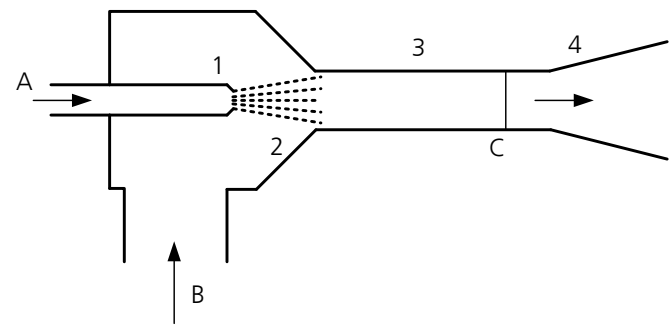

FIGURE 3: GENERAL SCHEME OF AN EJECTOR, DESCRIPTION IN TEXT

compressor. This is necessary to avoid water droplets from entering the second compressor and damaging its blades. With this constraint, the required mass flow rate of the water at the mixing point is defined.

3. EJECTOR MODEL DESCRIPTION

The principal design of a two-phase ejector is shown in Fig. 3. An ejector consists of four main parts, namely a primary nozzle (1), a suction chamber (2), a mixing chamber (3), and a diffuser (4). In the system under consideration, the motive (or primary) flow (A) enters the ejector at high-pressure in the sub-cooled liquid phase. The motive flow is accelerated in a convergent nozzle, usually causing a spray flow at the outlet. Via momentum transfer, this flow entrains the suction (or secondary) flow (B). Further momentum transfer from the liquid to the steam causes a supersonic shock (C) in the mixing chamber. This shock increases the pressure in the flow. A further gain in pressure is achieved by the deceleration in the diffuser. By comparing this configuration with the available ejector configurations in the literature, the ejector might be referred to as a two-phase condensing ejector, which is a novel utilization of ejectors firstly developed by Miguel and Brown [19]. They experimented with steam-salt water in underwater propulsion applications. Figure 4 shows a schematic of the ejector as stated in Miguel and Brown [19].

High pressure liquid is accelerated in the converging motive nozzle whereas, high velocity vapor gets entrained in the suction chamber. The two fluids reach the mixing chamber, where they mix, with relatively high velocity differences and different ther-

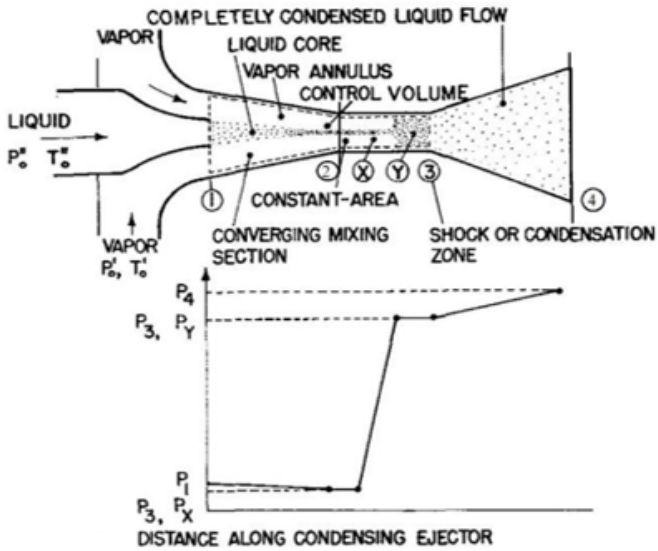

FIGURE 4: CONDENSING EJECTOR DEVELOPED BY MIGUEL AND BROWN [19]

modynamic states that could be utilized advantageously. Due to the high velocity difference, high vapor condensation rate happens within the ejector. This consequently results in a strong shock wave due to the change in density of the fluid streams. The shock wave produce a sharp pressure rise with complete condensation of the fluid streams. Miguel and Brown [19] have reported a complete liquid state at the diffuser outlet (section 4 in Fig. 4). Later Bergander [9] has developed a novel condensing ejector cycle utilizing the R22 refrigerant. Bergander [9] has reported through experimental attempts a COP improvement of 16 % over standard vapor compression system. Bergander [9] has argued though that improvements up to 38 % in COP could be achieved theoretically. However, the shock wave in Bergander [9] condensing ejector cycle did not result in a complete condensation of the mixing fluids. In fact depending on the operating conditions of the mixing fluids, relatively high vapor volume fractions can be achieved at the ejector's outlet.

As a matter of fact, what is desired in this paper, as will be shown later, is to achieve an outlet quality that is as high as possible. The ejector will be thus referred to only as a two-phase ejector. To the best of the authors knowledge, there is no model for a two-phase ejector with a highly super-heated suction flow and a super-sonic shock in the mixing tube. Therefore, an existing model for a two-phase ejector is adapted from the work of Šarevski and Šarevski [13]. The model proposed by them was modified to fit the ejector's application in the cycle proposed here. The equations for the ejector components are written in Modelica making a complete new ejector component, which was later connected and simulated with the other cycle components. Figure 5 shows the modeling procedure for the ejector.

Model Inputs. The ejector is simulated for a given set of inlet conditions for both the motive and suction fluids. The reason for this is to study the ejector performance for given initial conditions, which come as inputs from the available steam and condensate at the industrial plant. Constant efficiencies are proposed for the motive nozzle, suction nozzle, mixing chamber and diffuser.

Motive nozzle. A converging nozzle is chosen here to provide the maximum possible velocity at the nozzle exit and at the same time the lowest exit pressure. For the analysis, it is necessary to calculate the outlet velocity $c_{\mathrm{mn,out}}$ and the area at the motive nozzle exit $A_{\mathrm{mn,out}}$. From energy conversion, the exit velocity is a function of pressure difference across the nozzle and the specific volume of the fluid at the nozzle exit (see Eq.4 in Fig. 5). The pressure at the nozzle exit $p_{\mathrm{mn,out}}$ is equal to the mixing chamber pressure p_{mc}. The mixing chamber pressure is a free variable in the model and it is used as an optimization parameter for maximizing the pressure ratio over the ejector. Initial simulations have shown that a ratio between the mixing chamber pressure p_{mc} and the inlet pressure of the suction flow $p_{\mathrm{sn,in}}$ of about 0.95 lead to the highest pressure ratios over the ejector. Therefore, this value was fixed in the subsequent simulations. Since the motive fluid will be in the liquid state across the whole nozzle, the outlet specific volume $v_{\mathrm{mn,out}}$ can be calculated from water tables. The nozzle is simulated with an efficiency η_{mn} of 85 %.

Suction nozzle. The motive fluid expands and entrains the suction fluid into the mixing chamber. The pressure at the nozzle exit $p_{\mathrm{sn,out}}$ equals the mixing chamber pressure p_{mc}. The velocity of the fluid at the nozzle exit is calculated through energy conservation by using the enthalpy difference across the nozzle (see Eq.8 in Fig. 5). To get the nozzle exit area $A_{\mathrm{sn,out}}$, the specific volume at the nozzle exit $v_{\mathrm{sn,out}}$ is calculated as a function of exit pressure $p_{\mathrm{sn,out}}$ and enthalpy $h_{\mathrm{sn,out}}$. The nozzle is simulated with an efficiency η_{sn} of 85 %.

Mixing Chamber. The motive and suction fluids flow with large velocity difference, which results in the acceleration of the suction fluid. The mixing process is rather complex as a result of the interactions between the fluids. Assuming constant pressure mixing occurring inside the constant area mixing section, the pressures $p_{\mathrm{mc}} = p_{\mathrm{mn,out}} = p_{\mathrm{sn,out}}$ and the cross-sectional areas $A_{\mathrm{mn,out}} + A_{\mathrm{sn,out}} = A_{\mathrm{mc}}$. Therefore, using the momentum equation of the mixing chamber, the velocity of the combined flow can be calculated (Eq.10 in Fig. 5). The mixing chamber is simulated with an efficiency η_{mc} of 95 %.

Owing to the velocity difference between the motive and suction flow, the mixing process is the first source of thermodynamic irreversibility and exergy loss in the ejector. Using the energy equation of the mixing chamber, the enthalpy of the combined flow is calculated (Eq.14 in Fig. 5). The velocity of the combined flow is normally supersonic, which then causes the formation of a shock wave. In Fig. 5 two different subscripts are attached to the mixing chamber properties, i.e. bs and as. These refer to conditions occurring before the shock wave (bs) and after the shock wave (as) that occurs in the mixing chamber. In two-phase flow, this is accompanied by mass transfer from one phase to the other. In the current simulations the mass flow rate of the motive fluid ($\dot{m}_{\mathrm{mot}}$ or $\dot{m}_{\mathrm{mn}}$) is larger than that of the suction fluid ($\dot{m}_{\mathrm{suc}}$ or $\dot{m}_{\mathrm{sn}}$). This will cause the formation of a so called pseudo-shock wave, a feature for dominantly liquid two-phase flow [13]. To calculate the pressure raise across the shock wave, the sound velocity and the pseudo-isentropic exponent for the two-phase pseudo-fluid

are needed (Eq.15-19 in Fig. 5). To calculate the sound velocity of the two-phase flow, the square root of the derivative of pressure with respect to density at a constant entropy has been used, i.e. Eq. 15 in Fig. 5. Despite the pressure rise caused by the shock wave, it is a thermodynamically irreversible process, that results in an increase in entropy. The shock wave is considered the second main source of losses in the ejector.

Diffuser. The subsonic diffuser allows for additional compression. Using the diffuser efficiency, the outlet pressure at the diffuser exit can be obtained. The diffuser was simulated with an efficiency $\eta_{\mathrm{is,diff}}$ of 60 %.

Model Output. The output of the model is the ejector's pressure ratio Πej, which is the ratio of the ejector outlet pressure to the suction flow inlet pressure:

$$\Pi_{\mathrm{ej}} = p_{\mathrm{diff,out}}/p_{\mathrm{sn,in}} \tag{2}$$

Another important parameter to assess the performance of ejectors is the entrainment ratio w. This is the ratio between the suction fluid and the motive fluid mass flow rates. The ratio is given as:

$$w = \dot{m}_{\mathrm{suc}}/\dot{m}_{\mathrm{mot}} \tag{3}$$

In the modeling procedure there was a challenge to calculate the outlet pressure of the ejector. Generally, a two-phase mixture is expected at the exit of the ejector. To calculate that, the isentropic efficiency of the diffuser is needed to give the value of the outlet enthalpy and entropy of the two-phase fluid mixture at the diffuser exit. From these two properties the outlet pressure is calculated. Using the standard water medium in Modelica [16], four separate equations are provided to calculate the water pressure from enthalpy and entropy. The equations require that the phase region of water to be first defined to do the calculations. In the simulations, depending on the operating parameters, the outlet two-phase water-steam mixture can have a quality ranging from about 0.8 to almost zero. Therefore, the quality of the water-steam mixture at the diffuser inlet had to be checked each time to use the correct equation for calculating the outlet pressure. A simple optimization process was introduced where the mixture quality is first checked at the outlet of the mixing chamber. Afterwards, the region of water in the pT-diagram is determined followed by choosing the right corresponding equation to calculate the outlet pressure.

4. SIMULATED CYCLES, RESULTS AND DISCUSSIONS

In this section the results are presented and discussed. The two stages compression cycle with direct injection for simple intercooling will be first presented as a baseline case. The effect of various ejector parameters and its working conditions on the ejector's performance and that of the heat pump are subsequently studied. These parameters are the ejector's motive fluid pressure, p_{mot}, the mass flow rate of the motive fluid $\dot{m}_{\mathrm{mot}}$ and the compressor pressure ratio Π_{c}. Their consequent effect on the ejector's pressure ratio Π_{ej} and the overall heat pump COP are demonstrated. The section concludes with the comparison of the two cycles.

TABLE 2: TWO COMPRESSOR STAGES WITH DIRECT INJECTION

Direct injection	
Inlet conditions	$\dot{m}_{\mathrm{s}} = 1\,\mathrm{kg\,s^{-1}}$
	$p_{\mathrm{in}} = 1\,\mathrm{bar(a)}$
	$T_{\mathrm{in}} = 100\,^{\circ}\mathrm{C}$
Outlet pressure:	$p_{\mathrm{out}} = 2.57\,\mathrm{bar(a)}$
	$T_{\mathrm{out}} = 128\,^{\circ}\mathrm{C}$
Number of compressor stages:	2
Pressure ratio:	Stage 1: $\Pi_{\mathrm{c}} = 2.02$
	Stage 2: $\Pi_{\mathrm{c}} = 2.02$
Isentropic efficiency:	$\eta_{\mathrm{is,c}} = 70\,\%$
Electric power consumption:	Stage 1: $P_{\mathrm{c}} = 162\,\mathrm{kW}$
	Stage 2: $P_{\mathrm{c}} = 182\,\mathrm{kW}$
	$P_{\mathrm{p}} = 0.337\,\mathrm{kW}$
$\dot{Q}_{\mathrm{sink}}$:	2169 kW
COP:	5.975

4.1 Architecture 1: Two Compressor Stages with Direct Injection for Intercooling

An open two stage compression cycle with direct injection is used as a baseline for the simulations (see Fig. 1). As said, two de-superheaters are used to inject water at a pressure of 20 bar and a temperature of 90 °C in the main steam line. In the simulations, a value of the pressure drop caused by the de-superheater is needed to be given. Desuperheating can be realized through several possibilities, each having its own advantages and drawbacks. Furthermore, the chosen concept for de-superheating is applications relevant. Through contacts with de-superheaters manufacturers, a de-superhater was chosen based on a comprise of working conditions, de-superheating performance, device size and the resulting pressure drop. The pressure drop for the chosen de-superheater was in the range of 0.3 bar to 0.5 bar. The 0.5 bar pressure drop was used in the simulations. Moreover, 20 bar inlet pressure for water injection is chosen for a proper operation of the de-superheater. Besides, the liquid water mass flow rate through the de-superheater is controlled in such a way to ensure that the steam has a superheat of $\Delta T_{\mathrm{sup}} = 10\,\mathrm{K}$ and 0 K at the exit of first and second compressors, respectively (see Fig. 1). Table 2 shows the results of the baseline scenario.

From Table 2, it can be seen that through the use of two compressors each having a pressure ratio Π_{c} of about 2 the outlet pressure is 2.57 bar(a). The compressors each had an isentropic efficiency of 70 %, though the power required by the second compressor was 20 kW higher than that of the first one. The steam entering the second compressor is at a higher temperature and therefore density. Hence, to achieve the same pressure ratio, the second compressor would have to add more power in compressing the same amount of steam. Additionally, the power required by the pump is low and therefore it is neglected in the calculations.

4.2 Architecture 2: Compressor Stage with Ejector

A schematic of the compressor cycle with the ejector is shown in Fig. 2. Usually, the outlet of the ejector will be in the two-phase region and a separator is needed after the ejector to ensure that only dry steam is delivered to the industrial plant. The liquid

Inputs: $p_{mn,in}, p_{sn,in}, T_{mn,in}, T_{sn,in}, \dot{m}_{mn}, \dot{m}_{sn}, \eta_{mn}, \eta_{sn}, \eta_{mc}, \eta_{diff}$

Motive nozzle

$$h_{mn,out} = h_{mn,in} + \eta_{mn}\left(h_{mn,out,is} - h_{mn,in}\right) \text{ [Isentropic efficiency definition]} \quad (1)$$

$$\Delta p_{mn} = p_{mn,in} - p_{mn,out} \quad (2)$$

$$\upsilon_{mn,out} = f\left(p_{mn,out}, h_{mn,out}\right) \quad (3)$$

$$c_{mn,out} = \sqrt{2\Delta p_{mn,}\upsilon_{mn,out}} \text{ [Energy conservation]} \quad (4)$$

$$A_{mn,out} = (\dot{m}_{mn}\, \upsilon_{mn,out}) / c_{mn,out} \quad (5)$$

Suction nozzle

$$h_{sn,out} = h_{sn,in} + \eta_{sn}\left(h_{sn,out,is} - h_{sn,in}\right) \text{ [Isentropic efficiency definition]} \quad (6)$$

$$\upsilon_{sn,out} = f\left(p_{sn,out}, h_{sn,out}\right) \quad (7)$$

$$c_{sn,out} = \sqrt{2(h_{sn,in} - h_{sn,out})} \text{ [Energy conservation]} \quad (8)$$

$$A_{sn,out} = (\dot{m}_{mn}\, \upsilon_{sn,out}) / c_{sn,out} \quad (9)$$

Mixing chamber before the shock:

$$p_{mn,out}A_{mn,out} + \dot{m}_{mn}c_{mn,out} + p_{sn,out}A_{sn,out} + \dot{m}_{sn}\, c_{sn,out} = p_{mc,bs}A_{mc} + (\dot{m}_{mn} + \dot{m}_{sn})c_{mc,bs} \text{ [Momentum conservation]} \quad (10)$$

$$c_{mc,bs} = \eta_{mc}\,(m_{mn}\, c_{mn,out} + m_{sn}\, c_{sn,out}) \text{ [Isentropic efficiency definition]} \quad (12)$$

$$\text{where } m_{mn} = \dot{m}_{mn} / (\dot{m}_{mn} + \dot{m}_{sn}) \text{ and } m_{sn} = \dot{m}_{sn} / (\dot{m}_{mn} + \dot{m}_{sn}) \quad (13)$$

$$h_{mc,bs} = m_{mn}\, h_{mn,out} + m_{sn}\, h_{sn,out} + m_{mn}\frac{{c_{mn,out}}^2}{2} + m_{sn}\frac{{c_{sn,out}}^2}{2} - \frac{{c_{mc,bs}}^2}{2} \text{ [Energy conservation]} \quad (14)$$

Mixing chamber after the shock:

$$a_{cr} = \sqrt{(\Delta p/\Delta\rho)_{s=const}} \quad (15)$$

$$M_{bs} = c_{mc,bs}/\, a_{cr} \text{ and } M_{as} = c_{mc,as}/\, a_{cr} \quad (16)$$

$$M_{bs}\, M_{as} = 1 \quad (17)$$

$$\frac{p_{mc,as}}{p_{mc,bs}} = \frac{M_{bs}^2 - \frac{(\kappa-1)}{(\kappa+1)}}{1 - \frac{(\kappa-1)M_{bs}^2}{(\kappa+1)}} \text{ [pseudo-shock wave pressure raise]} \quad (18)$$

$$\text{where } \kappa = f(p_{mc}, h_{mc}) \quad (19)$$

$$h_{mc,as} = \frac{c_{mc,as}^2}{2} \quad (20)$$

$$s_{mc,as} = f(p_{mc,as}, h_{mc,as}) \quad (21)$$

Diffuser:

$$\eta_{diff} = \frac{\Delta h_{rdin}}{(c_{mc,as}^2/2)}, \text{where } \Delta h_{rdin} = h_{diff,out,is} - h_{mc,as} \quad (22)$$

$$h_{diff,out} = h_{mc,as} + \left(h_{diff,out,is} - h_{mc,as}\right)/\, \eta_{diff} \text{ [Isentropic efficiency definition]} \quad (23)$$

$$p_{diff,out} = f(h_{diff,out}, s_{mc,as}) \quad (24)$$

Output: Π_{ej}

*

FIGURE 5: MODELING PROCEDURE FOR THE EJECTOR

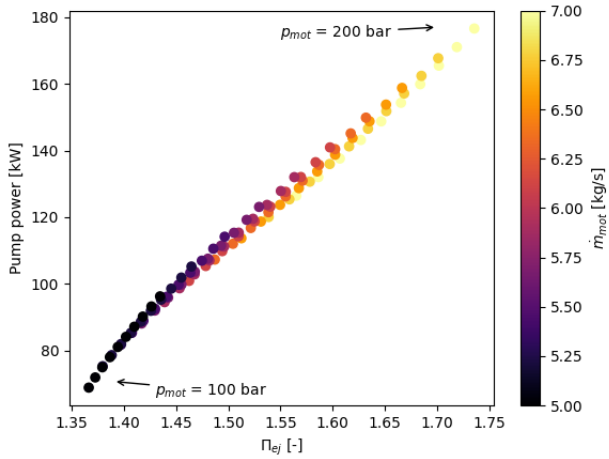

FIGURE 6: Π_{ej} AGAINST THE P_p, p_{mot} VARIED FROM 100 bar **TO** 200 bar, **$\dot{m}_{mot}$ VARIED FROM** 5 kg s^{-1} **TO** 7 kg s^{-1} **AND Π_c = 2.5**

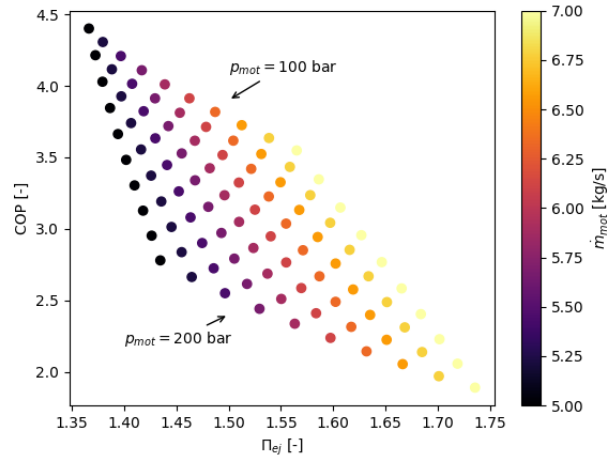

FIGURE 7: Π_{ej} AGAINST THE COP, p_{mot} VARIED FROM 100 bar **TO** 200 bar, **$\dot{m}_{mot}$ VARIED FROM** 5 kg s^{-1} **TO** 7 kg s^{-1} **AND Π_c = 2.5**

fraction, i.e. the condensate, is directed to a mixing point before the motive fluid pump, increasing the temperature of the pumped liquid. As previously mentioned, condensate at 90 °C is used as a motive fluid.

Parameter variations. To see the effect of working parameters on the ejector's performance, the pressure of the motive fluid p_{mot} was varied between 100 bar to 200 bar. Simultaneously, the amount of condensate directed before the pump was controlled to change the mass flow rate of the motive fluid $\dot{m}_{mot}$ from 5 kg s^{-1} to 7 kg s^{-1}. The compressor pressure ratio Π_c was kept constant at 2.5 and the respective steam flow rate through the compressor was fixed at a rate of 1 kg s^{-1}. The effect of changing the $\dot{m}_{mot}$ and p_{mot} on the Π_{ej} is shown in Fig. 6. The p_{mot} is changed during the simulations in steps of 10 bar. It can be seen that higher flow rates and pressures lead to higher ejector's pressure ratios, but at the cost of a higher pumping power.

Actually, during the simulations lower values of motive pressures and flow rates were indeed simulated. It was noted that the ejector will not work under these conditions. Higher values of pressures and flow rates are needed to accelerate the motive flow, which in turns needs to expand and entrain the suction flow. Lower values of motive fluid pressures or mass flow rates will not cause enough expansion to entrain the suction flow into the mixing chamber, i.e. the motive flow will not have enough potential energy. The design point happens at a narrow range of operating parameters that will result in a perfect condition for the creation of the shock wave. This is consequently needed to increase the mixture pressure. Changing the operating parameters below and above the design parameter will cause the ejector to malfunction. This results here in limiting the entrainment ratio w to values below 0.3 and p_{mot} to values above 100 bar.

Another study is shown in Fig. 7 where the ejector's pressure ratio Π_{ej} is plotted against the COP while again varying $\dot{m}_{mot}$ and p_{mot} as done in the previous analysis. From the figure, it can be seen that higher cycle COPs are interestingly achieved at lower values of Π_{ej}, $\dot{m}_{mot}$ and p_{mot}.

A possible reason for the behavior seen in Fig. 7 might be related to the exit quality of the two-phase fluid x_{ej}. Even though, the Π_{ej} was high, the value of the outlet quality of the two-phase mixture was low at these points. Therefore, the amount of heat delivered to the industrial plant is low resulting in low values of COPs. This can be seen more clearly in Fig. 8 where the amount of heat delivered $\dot{Q}_{sink}$ is shown for the case of Π_c = 2.5.

A possible explanation for having higher $\dot{Q}_{sink}$ at low ejector's pressure ratio can be related to what was earlier said in the ejector model description. Looking at Fig. 8 more in detail, it is seen that $\dot{Q}_{sink}$ of about 1400 kW is achieved at $\dot{m}_{mot}$ of 5 kg s^{-1}, p_{mot} of 100 bar and Π_{ej} of around 1.36. The motive fluid in this case does not have as high potential energy as it would have if it enters the nozzle with p_{mot} of 200 bar and $\dot{m}_{mot}$ of 7 kg s^{-1}. Thus, the resulting expansion of the motive fluid and the consequent momentum, energy and mass exchange in the mixing chamber would not be high as it would be with p_{mot} of 200 bar and $\dot{m}_{mot}$ of 7 kg s^{-1}. As a consequence, the resulting shock wave would be weaker and therefore, the vapor condensation rate. The two-phase mixture would leave after the shock wave with lower pressure rise due to a weak shock but, with a higher quality. Hence, the amount of heat delivered to the heat sink and the consequent COP would be higher.

Compressor Pressure Ratio. The pressure ratio of the compressor Π_c was changed in the simulations to see its effect on the both the ejector and the cycle performance. The compressor was simulated with an isentropic efficiency η_{is} of 70 %. Figure 9 shows the cycles COPs using three values of Π_c, namely, 1.7, 2.1 and 2.5. The values of $\dot{m}_{mot}$ and p_{mot} were changed in each simulation as in the previous analyses. Figure 9 shows that the COPs changes in slightly different trend with each compression ratio with lower values of Π_c resulting in a higher values of COPs.

Looking at Fig. 9 more in detail, it can be seen that as the compression ratio decreases the curves gets narrower and the COPs increases. The Left figure (with Π_c = 2.5) shows a maximum COP of 4.3 at a p_{mot} of 100 bar and $\dot{m}_{mot}$ of 5 kg s^{-1}. On

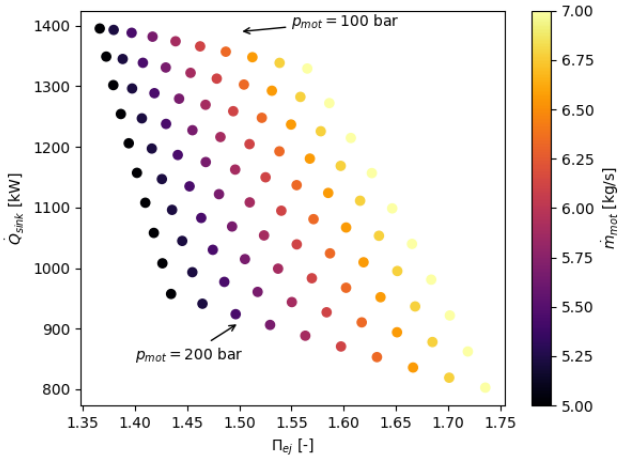

FIGURE 8: HEAT FLOW TO THE INDUSTRIAL PLANT, p_{mot} VARIED FROM 100 bar **TO** 200 bar, **$\dot{m}_{mot}$ VARIED FROM** 5 kg s^{-1} **TO** 7 kg s^{-1} **AND Π_c = 2.5**

the other side, the right figure (with $\Pi_c = 1.7$) shows a maximum COP of 7.8 at the same p_{mot} and $\dot{m}_{mot}$. A possible explanation for this would be that although higher compressor pressure ratios would give higher outlet pressure nevertheless, the outlet temperature, and at the same time the outlet density, would be higher. Therefore, the compressor would have to do more work in compressing the steam to higher temperatures which will lead to a lower cycle COP.

Architectures Comparison. The two architectures are compared to each others at two operating points. The two points conditions along with the simulations results are shown in Table 3 and Table 4 respectively. The two architectures were compared on the basis of delivering the same amount of heat $\dot{Q}_{sink}$ at the same outlet temperature and pressure. Looking at the results in Table 3 first, it can be seen that by using an ejector, the same outlet conditions were achieved without the use of a second compressor. This has caused an increase of about 11 % in the COP in comparison to the direct injection cycle with the de-superheater. The positive displacement pump was used to pump water to 120 bar at the inlet of the ejector motive nozzle. This results in a pump power of 77 kW considering that the pump was simulated with an efficiency $\eta_{is,p}$ of 80 %. The value of this efficiency was based on local pump manufacturer [18]. Additionally, as can be seen from Table 3, the mass flow rate through the direct injection cycle was changed to achieve the same amount of $\dot{Q}_{sink}$ as the ejector cycle. On the other side, if the simulations were done again using higher a compressor efficiency of 80 % and a lower pump efficiency of 70 %, then the total increase in the COP under the same conditions through the use of an ejector will be around 4 %. This can still be considered a good improvement considering that the use of an ejector has resulted in saving a second complex compressor stage.

Table 4 shows the case where a temperature above 150 °C was achieved by the two architectures. In this case, the ejector cycle had a lower COP compared to the direct injection cycle. Both cycles delivered the same amount of $\dot{Q}_{sink}$ at the same outlet temperature and pressure. Again, the mass flow rate through the direct injection cycle was reduced to match the $\dot{Q}_{sink}$ delivered by the ejector cycle. Both cycles were simulated with a compressor efficiency of 70 % and a pump efficiency of 80 %. It can be noticed from Table 4 that the inlet steam conditions were changed to 2 bar(a) at a saturation temperature of 121 °C. During the simulations, it was difficult to achieve a temperature above 150 °C using saturated steam at 1 bar(a) at the inlet conditions. This would require an additional compressor stage in each architectures which was avoided to not increase the complexity of the cycle's structures.

During the simulations of the two above-mentioned operating points, several interesting behaviors were noticed. It was first thought that using a higher compression ratio in the ejector cycle with higher outlet temperature would results in a two-phase exit mixture of a higher quality and temperature. However, increasing the temperature and the pressure of the suction flow, i.e. the conditions at the outlet of the compressor, would result in the formation of a strong shock wave in the ejector's mixing section. The strength of the shock is indicated by noticing the difference of the Mach number before and after the shock wave. Higher suction flow inlet temperatures and pressures results in a higher mach number differences thereby causing a strong shock wave. The model shows that the stronger the shock is, the more condensation of the flow would occur and the lower the outlet quality at the exit. Thus the cycle's COP would be lower.

Second, even though the COP in Table 4 was less in the ejector cycle, the use of an ejector may still be promising to achieve temperatures above 150 °C. Steam compressors with high pressure ratios are very complex in the design and expensive in the manufacturing [2]. This comes especially true for the second compressor that will need to compress steam with a higher inlet pressure and a higher inlet density. Most probably a third compression stage would be required to achieve such a temperature with direct injection. Hence, the results indicate that a properly designed ejector, can provide temperatures above 150 °C with only one compressor. Thus resulting in saving a second and maybe even a third complex compression stages.

5. OUTLOOK AND CONCLUSION

Though the results presented in the previous section looks promising for the applications of two-phase water ejector in HTHPs, several challenges still need to be solved. Although the model used in this paper was made and verified by Šarevski and Šarevski [13], it has not been verified for the use of two-phase water at such operating parameters. This comes particularly considering the fact that the model was edited and optimized to results in good ejector performance under the operating parameters examined in this study. Still, the first simulations results done here have shown a high promising potential for the ejector to enhance the performance of HTHPs. The next step would be to extend the model into a detailed 1-D model that also takes into account the ejector geometry in detail. The geometrical design of the motive nozzle, the mixing section and the diffuser have to be optimized for a better performance of the ejector. Though, 1-D models for ejectors are available in literature, a detailed model for two-phase

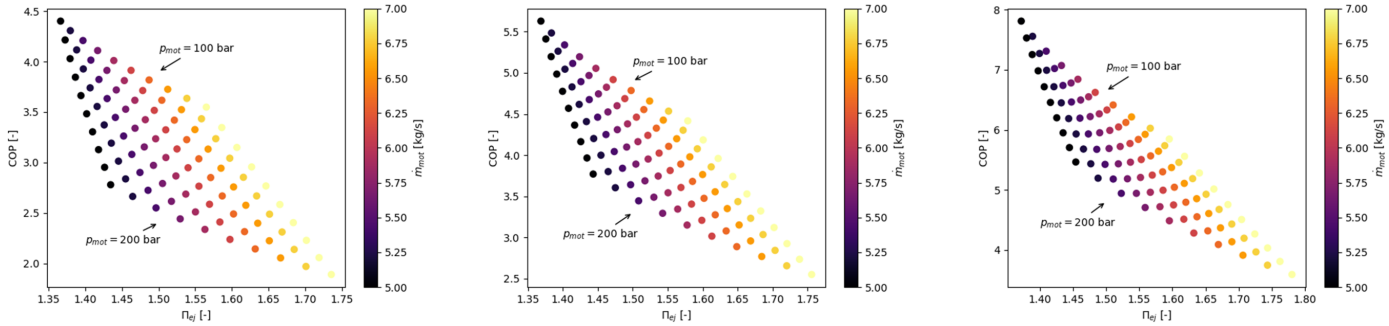

FIGURE 9: EJECTOR CYCLE COPs FOR DIFFERENT Π_c, p_{mot} VARIED FROM 100 bar **TO** 200 bar**, $\dot{m}_{mot}$ VARIED FROM** $5\,\mathrm{kg\,s^{-1}}$ **TO** $7\,\mathrm{kg\,s^{-1}}$**. Π_c LEFT = 2.5, MIDDLE Π_c = 2.1, RIGHT Π_c = 1.7**

TABLE 3: OPERATING CONDITIONS OF THE TWO ARCHITECTURES

	Direct injection	Ejector cycle
Inlet conditions	$\dot{m}_s = 0.71\,\mathrm{kg\,s^{-1}}$	$\dot{m}_s = 1\,\mathrm{kg\,s^{-1}}$
	$p_{in} = 1\,\mathrm{bar(a)}$	$p_{in} = 1\,\mathrm{bar(a)}$
	$T_{in} = 100\,°\mathrm{C}$	$T_{in} = 100\,°\mathrm{C}$
Outlet pressure:	$p_{out} = 2.57\,\mathrm{bar(a)}$	$p_{out} = 2.57\,\mathrm{bar(a)}$
	$T_{out} = 128\,°\mathrm{C}$	$T_{out} = 128\,°\mathrm{C}$
Number of compressor stages:	2	1
Pressure ratio:	Stage 1: $\Pi_c = 2.02$	$\Pi_c = 1.7$
	Stage 2: $\Pi_c = 2.02$	
Isentropic efficiency:	$\eta_{is,c} = 70\%$	$\eta_{is,c} = 70\%$
Electric power consumption:	Stage 1: $P_c = 115\,\mathrm{kW}$	$P_c = 139\,\mathrm{kW}$
	Stage 2: $P_c = 129\,\mathrm{kW}$	
	$P_p = 0.232\,\mathrm{kW}$	$P_p = 77\,\mathrm{kW}$
$\dot{Q}_{sink}$:	1544 kW	1544 kW
COP:	5.977	6.652

TABLE 4: OPERATING CONDITIONS OF THE TWO ARCHITECTURES ABOVE 150 °C

	Direct injection	Ejector cycle
Inlet conditions	$\dot{m}_s = 0.54\,\mathrm{kg\,s^{-1}}$	$\dot{m}_s = 1\,\mathrm{kg\,s^{-1}}$
	$p_{in} = 2\,\mathrm{bar(a)}$	$p_{in} = 2\,\mathrm{bar(a)}$
	$T_{in} = 121\,°\mathrm{C}$	$T_{in} = 121\,°\mathrm{C}$
Outlet pressure:	$p_{out} = 5\,\mathrm{bar(a)}$	$p_{out} = 5\,\mathrm{bar(a)}$
	$T_{out} = 153\,°\mathrm{C}$	$T_{out} = 153\,°\mathrm{C}$
Number of compressor stages:	2	1
Pressure ratio:	Stage 1: $\Pi_c = 1.79$	$\Pi_c = 1.7$
	Stage 2: $\Pi_c = 1.79$	
Isentropic efficiency:	$\eta_{is,c} = 70\%$	$\eta_{is,c} = 70\%$
Electric power consumption:	Stage 1: $P_c = 77\,\mathrm{kW}$	$P_c = 145\,\mathrm{kW}$
	Stage 2: $P_c = 86\,\mathrm{kW}$	
	$P_p = 0.146\,\mathrm{kW}$	$P_p = 62\,\mathrm{kW}$
$\dot{Q}_{sink}$:	1148 kW	1148 kW
COP:	6.673	5.178

water ejector for HTHPs application is still missing.

This paper has examined the performance of two-phase water ejector in HTHPs. A thermodynamic model of an ejector was optimized and implemented in an open heat pump cycle model. Several operating parameters were changed to find their effect on the ejector and the total cycle performance. It was seen that the motive fluid pressure and the motive fluid flow rate have a significant effect on the pressure ratio achieved by the ejector. For a proper operation, inlet pressures of 100 bar and above are needed at the motive nozzle inlet of the ejector. The entrainment ratio on the other side should be lower than about 0.3 to ensure a significant pressure increase at the outlet of the ejector with a good outlet quality. The ejector cycle was compared to two stages compressor cycle with direct injection for intermediate cooling. It was found that the ejector can function as a second step compression thereby increasing the COP of the cycle by about 10 %.

REFERENCES

[1] de Boer, Robert, Marina, Andrew, Zühlsdorf, Benjamin, Arpagaus, Cordin, Bantle, Michael, Wik, Veronika, Elmegaard, Brian, Corberan, Jose M and Benson, Jessica. "Strengthening Industrial Heat Pump Innovation: Decarbonizing Industrial Heat." (2020).

[2] Arpagaus, Cordin, Bless, Frédéric, Uhlmann, Michael, Schiffmann, Jürg and Bertsch, Stefan S. "High temperature heat pumps: Market overview, state of the art, research status, refrigerants, and application potentials." *Energy* Vol. 152 (2018): pp. 985–1010.

[3] Finger, Stephan and Abu Khass, Omar. "The DLR High Temperature Heat Pump Pilot Plants." 2021. European Heat Pump Summit, Nuremberg.

[4] Zühlsdorf, Benjamin, Schlemminger, Christian, Bantle, Michael, Evenmo, Kjetil and Elmegaard, Brian. "Design recommendations for R-718 heat pumps in high temperature applications." *Proceedings of the 13th IIR Gustav Lorentzen Conference,Valencia*. 2018. International Institute of Refrigeration (IIR).

[5] Power, Robert B. *Steam jet ejectors for the process industries*. New York, NY (United States); McGraw-Hill (1994).

[6] Besagni, Giorgio, Mereu, Riccardo and Inzoli, Fabio. "Ejector refrigeration: A comprehensive review." *Renewable and Sustainable Energy Reviews* Vol. 53 (2016): pp. 373–407.

[7] Tashtoush, Bourhan M, Moh'd A, Al-Nimr and Khasawneh, Mohammad A. "A comprehensive review of ejector design, performance, and applications." *Applied Energy* Vol. 240 (2019): pp. 138–172.

[8] Alam, Md Muntasir and Elbel, Stefan. "Utilization of Ejector for Decrease of Compressor Discharge Pressure in HVAC&R Applications." *Paper 2365*. 2022. International Refrigeration and Air Conditioning Conference, Purdue.

[9] Bergander, Mark J. "Refrigeration cycle with two-phase condensing ejector." *Paper 748*. 2006. International Refrigeration and Air Conditioning Conference, Purdue.

[10] Elbel, Stefan and Hrnjak, Predrag. "Ejector refrigeration: an overview of historical and present developments with an emphasis on air-conditioning applications." *Paper 884*. 2008. International Refrigeration and Air Conditioning Conference, Purdue.

[11] Šarevski, Milan N and Šarevski, Vasko N. "Preliminary study of a novel R718 refrigeration cycle with single stage centrifugal compressor and two-phase ejector." *International journal of refrigeration* Vol. 40 (2014): pp. 435–449.

[12] Šarevski, VN and Šarevski, MN. "Energy efficiency of the thermocompression refrigerating and heat pump systems." *International journal of refrigeration* Vol. 35 No. 4 (2012): pp. 1067–1079.

[13] Šarevski, Milan N and Šarevski, Vasko N. *Water (R718) turbo compressor and ejector refrigeration/heat pump technology*. Butterworth-Heinemann (2016).

[14] "The Modelica Association — Modelica Association." (2022). URL https://modelica.org. [Online; accessed 11. Dec. 2022].

[15] "Modelon Impact Platform." (2022). URL https://modelon.com/modelon-impact. [Online; accessed 11. Dec. 2022].

[16] "Modelica.Media.Water.StandardWater." (2021). URL https://doc.modelica.org/Modelica%203.2.3/Resources/helpMapleSim/Media/Water/StandardWater/index.html. [Online; accessed 25. Dec. 2022].

[17] Bühler, Fabian, Zühlsdorf, Benjamin, Nguyen, Tuong-Van and Elmegaard, Brian. "A comparative assessment of electrification strategies for industrial sites: Case of milk powder production." *Applied Energy* Vol. 250 (2019): pp. 1383–1401.

[18] "Hochdruckpumpen - SPECK Pumpen." (2022). URL https://www.speck-pumps.com/de/pc/speck/industrietechnik/hochdruckpumpen/?v=3a52f3c22ed6. [Online; accessed 25. Dec. 2022].

[19] Brown, George A. and Miguel, John. "An analytical and experimental investigation of a condensing ejector with a condensable vapor." *AIAA Paper No. 64-469, Washington, D.C. 1964*.